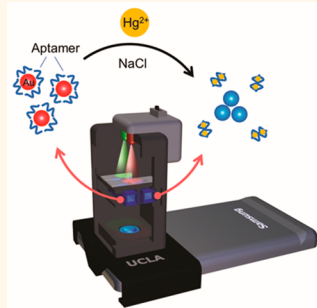


# Detection and Spatial Mapping of Mercury Contamination in Water Samples Using a Smart-Phone

Qingshan Wei,<sup>†,‡,§</sup> Richie Nagi,<sup>||,#</sup> Kayvon Sadeghi,<sup>†,‡,§</sup> Steve Feng,<sup>†</sup> Eddie Yan,<sup>†</sup> So Jung Ki,<sup>⊥</sup> Romain Caire,<sup>†</sup> Derek Tseng,<sup>†</sup> and Aydogan Ozcan<sup>†,‡,§,\*</sup>

<sup>†</sup>Electrical Engineering Department, <sup>‡</sup>Bioengineering Department, <sup>§</sup>California NanoSystems Institute (CNSI), <sup>||</sup>Department of Physics & Astronomy, and <sup>⊥</sup>Department of Chemistry and Biochemistry, University of California, Los Angeles (UCLA), Los Angeles, California 90095, United States. <sup>#</sup>R. Nagi and K. Sadeghi contributed equally to this project.

**ABSTRACT** Detection of environmental contamination such as trace-level toxic heavy metal ions mostly relies on bulky and costly analytical instruments. However, a considerable global need exists for portable, rapid, specific, sensitive, and cost-effective detection techniques that can be used in resource-limited and field settings. Here we introduce a smart-phone-based hand-held platform that allows the quantification of mercury(II) ions in water samples with parts per billion (ppb) level of sensitivity. For this task, we created an integrated opto-mechanical attachment to the built-in camera module of a smart-phone to digitally quantify mercury concentration using a plasmonic gold nanoparticle (Au NP) and aptamer based colorimetric transmission assay that is implemented in disposable test tubes. With this smart-phone attachment that weighs <40 g, we quantified mercury(II) ion concentration in water samples by using a two-color ratiometric method employing light-emitting diodes (LEDs) at 523 and 625 nm, where a custom-developed smart application was utilized to process each acquired transmission image on the same phone to achieve a limit of detection of ~3.5 ppb. Using this smart-phone-based detection platform, we generated a mercury contamination map by measuring water samples at over 50 locations in California (USA), taken from city tap water sources, rivers, lakes, and beaches. With its cost-effective design, field-portability, and wireless data connectivity, this sensitive and specific heavy metal detection platform running on cellphones could be rather useful for distributed sensing, tracking, and sharing of water contamination information as a function of both space and time.



**KEYWORDS:** smart-phone sensor • mercury detection • colorimetric sensor • gold nanoparticles • aptamers

Since the recognition of severe neurotoxic effects of mercury in the 1960s,<sup>1–3</sup> the development of detection techniques for real-time and long-term monitoring of mercury contamination in environmental and biological samples has become a high priority. Various neurological effects of mercury exposure have been mainly attributed to the organic form of mercury, predominantly methylmercury ( $\text{MeHg}^+$ ), which is known to accumulate in the food chain<sup>4</sup> and cross the blood–brain barrier after human ingestion.<sup>5,6</sup> While such findings have added weight to the severity of organic mercury contamination, the threat of inorganic mercury, namely, mercury(II) ions ( $\text{Hg}^{2+}$ ), should not be underestimated. In fact, mercury(II) ions are the primary mercury contamination in the aquatic system and the “precursor” form of methylmercury due to bacteria-assisted biotransformation processes.<sup>7,8</sup> Furthermore, inorganic mercury is known to be more nephrotoxic

than its organic form, as it primarily accumulates in the kidney proximal tubule cells.<sup>9</sup> Therefore, the detection and quantification of mercury(II) ion contamination in water systems are of paramount importance and could potentially be used to assist prevention of mercury ions from entering the food chain.

Toward this need, low nanomolar (nM) concentrations of mercury(II) ions have been traditionally detected by using spectroscopic methods, including, for example, atomic absorption spectroscopy (AAS),<sup>10,11</sup> inductively coupled plasma mass spectrometry (ICP-MS),<sup>12</sup> and atomic fluorescence spectrometry (AFS).<sup>13</sup> However, these approaches require complex sample preparation procedures, expensive and bulky instruments, and professionally trained personnel running the tests. Therefore, they are not well suited for rapid on-site detection of mercury and may not even be available for use in developing countries. On the other hand, recent advances

\* Address correspondence to ozcan@ucla.edu.

Received for review December 24, 2013  
and accepted January 19, 2014.

Published online January 20, 2014  
10.1021/nn406571t

© 2014 American Chemical Society

in microfabrication and nanoscience have enabled the development of portable detection assays that are integrated with lab-on-a-chip platforms, showing great potential for use in resource-limited environments.<sup>14–18</sup> Among these technologies, gold nanoparticle (Au NP)-based colorimetric assays are emerging as alternative approaches for heavy metal detection,<sup>19–21</sup> providing high sensitivity, specificity, and ease of signal read-out using, for example, UV-vis spectrometers<sup>19–21</sup> or glass slide readers.<sup>14</sup> However, these existing systems that utilize NPs are still limited due to their relatively bulky instrumentation, higher costs, and lack of wireless connectivity, which are important especially for distributed sensing and spatiotemporal mapping of contamination in remote locations and field settings. As an alternative to Au NP-based plasmonic techniques, detection of subppm levels of mercury(II) ions has recently been demonstrated by using dye-embedded polymer films as colorimetric substrates that are digitized using, for example, smart-phone cameras.<sup>22</sup> However, this recent approach does not utilize the processing/computational power of the phone, and it has limited detection sensitivity and repeatability due to unavoidable variations in ambient light conditions and user operation and/or alignment during the image capture process.

To provide a field-portable, cost-effective, and wirelessly connected platform to sensitively quantify heavy metal ion concentration in water samples, here we report a battery-powered mobile sensing device that consists of a lightweight (~37 g) opto-mechanical attachment to a smart-phone along with a custom-developed Android application for quantification, reporting, and sharing of detection results. This lab-on-a-phone device is based on dual-wavelength illumination using light-emitting diodes (LEDs) at 523 and 625 nm and can quantify mercury-induced subtle transmission changes of a colorimetric assay utilizing citrate-stabilized plasmonic Au NPs and aptamers (Apt) mixed within disposable test tubes. Due to the shift in the plasmonic resonance wavelength of dispersed and aggregated Au NPs in response to mercury(II) ions, we demonstrated sensitive detection of mercury contamination in water samples with a limit of detection (LOD) of ~3.5 ppb, which has the same order of magnitude as the maximum contaminant level (MCL) of mercury(II) recommended for drinking water, *i.e.*, 2 and 6 ppb, as established by the U.S. Environmental Protection Agency (EPA) and the World Health Organization (WHO), respectively.<sup>23,24</sup> With this cellphone-based colorimetric detection platform, we also demonstrated geospatial mapping of mercury(II) contamination in California by testing water samples collected at more than 50 locations, from tap water sources as well as natural sources such as rivers, lakes, and beaches. This heavy metal detection system running on smart-phones could provide a complementary addition to

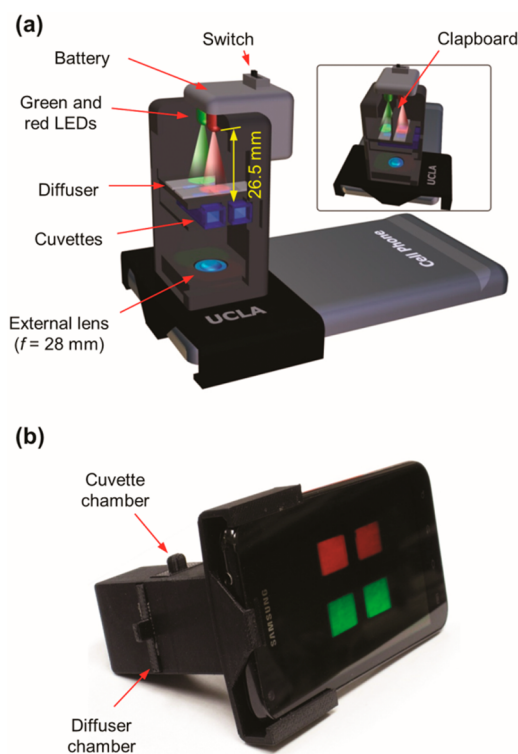


**Figure 1.** Design of the ratiometric optical reader on a smart-phone. (a) 3D schematic illustration of the internal structure of the opto-mechanical attachment. The inset image shows the same attachment with a slightly different observation angle. (b) Photograph of the actual optical reader installed on an Android-based smart-phone. The screen of the smart-phone displays a typical image of the sample and control cuvettes when illuminated by red (625 nm) and green (523 nm) LEDs simultaneously.

other mobile-phone-based imaging, sensing, and diagnostics devices<sup>25–42</sup> and holds significant potential for distributed sensing and spatiotemporal mapping and monitoring of mercury contamination globally. In fact, cellphone subscriptions worldwide have reached more than 7 billion by the end of 2013, and smart-phone penetration rate is globally increasing, which is estimated to reach more than 60%, 45%, and 25% by the end of 2015 in North America, Europe, and Africa, respectively.<sup>43</sup> Therefore, the use of mobile phones for bioanalytical measurement science as well as for reporting and sharing of results provides widely scalable, cost-effective, and yet rather powerful/competitive solutions to implement various tests and measurements even in resource-limited and field settings, which constitutes an important motivation for this work.

## RESULTS AND DISCUSSION

### Optical Design of the Smart-Phone-Based Mercury Reader.

We created an optical imaging interface that is mechanically attached to the existing camera module of a smart-phone to quantify mercury concentration using a colorimetric nanoparticle and aptamer assay.

This attachment contains two button cells (3 V), which are used to power two LEDs, as illustrated in Figure 1a. These LEDs are mounted at a sufficiently large distance (~26.5 mm) away from the location of the rectangular test tubes (containing the sample and control solutions) and are scattered by optical diffusers to ensure uniform illumination of both tubes (Figure 1a). The emission wavelengths of these LEDs were selected to be 523 and 625 nm to follow the shift in the extinction wavelengths of the dispersed and aggregated Au NPs, respectively. In order to obtain multispectral information from a given water sample, the green LED illuminated the bottom half while the red LED illuminated the top half of each cuvette (Figure 1a). To avoid a possible crosstalk between the green and red lights, the optical paths of the two LEDs were separated by an opaque clapboard before they reached the cuvettes (Figure 1a, inset) and passed through two rectangular apertures (6.6 × 5 mm, one for each color) that are placed in front of each cuvette. The transmitted light through the sample and control cuvettes was then collected through two other rectangular apertures of the same size to be imaged onto the digital camera of the smart-phone using a plano-convex lens ( $f = 28$  mm) (Figure 1a). This external lens was chosen to yield a demagnification factor of  $7 \times$  so that the two 6.6-mm-wide sample cuvettes could be simultaneously imaged within the active area of the smart-phone CMOS imager chip. All of these electrical and optical elements were consolidated in an opaque cuboid (Figure 1a, gray part) and coupled to a base plate (Figure 1a, black part) with a total weight of ~37 g. Although the current attachment is designed for an Android phone (Samsung Galaxy S II, Figure 1b), the same optical reader can be implemented on other smart-phones such as an iPhone, after slight mechanical modifications in the base attachment.

**Plasmonic Colorimetric Assay and Measurement of Mercury(II) Ion Concentration.** Spherical Au NPs have been previously studied as novel sensing probes for mercury(II) ion detection.<sup>19–21</sup> The characteristic color change of Au NPs from red to purple or blue upon aggregation that is induced by mercury(II) ion binding events constitutes the basis of the Au NP-based colorimetric detection assay. However, most Au NP-based probes require a surface modification step to conjugate mercury(II)-specific ligands onto Au NPs, and the LOD varies based on the capturing ligand that is selected.<sup>44–48</sup> Here, we adopt an alternative approach, which utilizes the strong affinity of the thymine-rich aptamer sequence to mercury(II) ions and citrate-stabilized Au NPs as colorimetric signal transducers to generate a high detection sensitivity.<sup>49</sup> In this protocol, Au NPs are used *without* the need for surface functionalization steps, which greatly facilitates field use. In a typical mercury detection experiment, 0.64 nM Au NPs (50 nm diameter) are mixed with 3 μM aptamer (5'-TTTTTTTTT-3') in 20 mM Tris-HCl buffer

(pH 8.0) to form the probe solution. Next, 4 μL of water sample solution is added to the probe solution and incubated for 5–10 min (see Methods section for details). Aptamer forms a protective layer on the surface of Au NPs, which prevents them from aggregation even in a high-salt environment such as 10 mM NaCl. However, this aptamer layer will be stripped off by the presence of mercury(II) ions due to the formation of more stable T-Hg<sup>2+</sup>-T complexes.<sup>50,51</sup> As a result, the unprotected Au NPs can undergo distinct color transition from red to blue in the presence of NaCl (Figure 2a), and this spectral shift is detected to quantify mercury concentration using our dual-wavelength smart-phone-based colorimetric reader.

A representative smart-phone-captured image of Au NP probe solutions with and without mercury(II) ions is depicted in Figure 2b. Each cuvette was illuminated by red and green LEDs at different spatial locations and separated by two rectangular apertures that are 3 mm apart from each other (Figure 2b). The illumination spots of the LEDs were sufficiently large to cover both the sample and control cuvettes (2 mm apart). This dual-illumination color and dual-cuvette configuration forms four readable signals in a single image frame, namely, red control (RC), red sample (RS), green control (GC), and green sample (GS) signals (Figure 2c). To quantify the mercury contamination in a given water sample, the acquired transmission image of these cuvettes (sample and control) is first digitally split into red (R) and green (G) channels (Figure 2c) to further minimize the spectral crosstalk between these two colors. The centroids of each rectangular aperture are automatically localized by a detection algorithm, and a rectangular region of interest (ROI, 400 × 300 pixels) around each of these four centroids is then used to calculate the averaged transmission signal for each ROI, yielding RC, RS, GC, and GS signals. Note that RC and RS are calculated using the red channel image, whereas GC and GS are calculated using the green channel image, both of which are digitally separated from the raw RGB image captured by the cellphone camera sensor (Figure 2c). The transmission intensity of the sample cuvette is further normalized to that of the control cuvette by placing two identical deionized water samples in both cuvette positions, leading to an illumination normalization factor of 1.15 for the red LED (R\_Factor) and 0.98 for the green LED (G\_Factor). The calibration ratio of the control cuvette (G/R\_C) was obtained by taking the ratio of the GC and RC. Similarly, the calibration ratio of the sample cuvette (G/R\_S) was obtained by taking the ratio of GS × G\_Factor to RS × R\_Factor. Finally, the ultimate normalized green-to-red signal (*i.e.*, normalized G/R) for a given water sample was computed by taking the ratio of G/R\_S to G/R\_C (Figure 2c). These calculations are automatically implemented using a custom-designed Android application running on

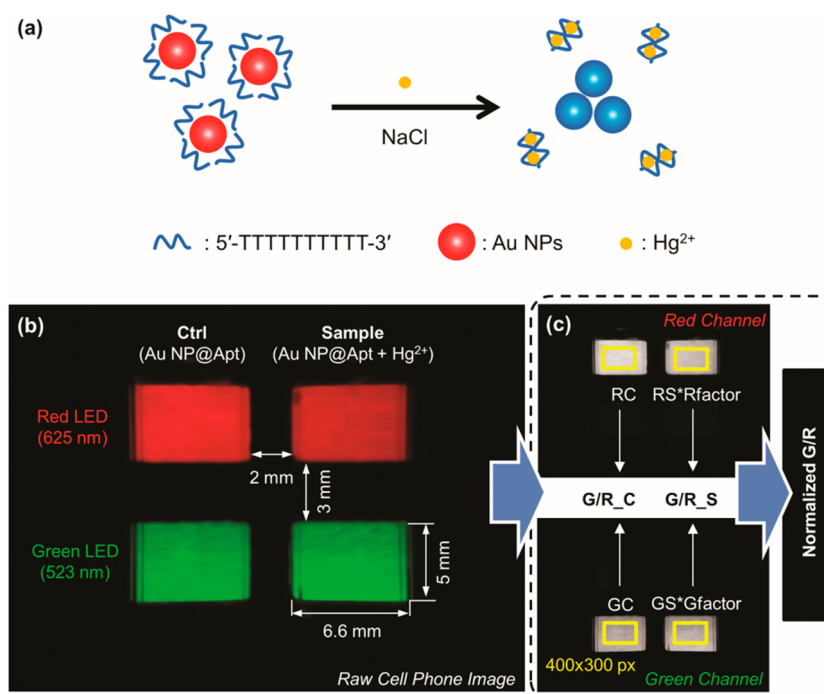


**Figure 2. Principle of dual-color dual-cuvette colorimetric detection.** (a) Scheme of the mercury sensing mechanism by using plasmonic Au NPs and aptamer. (b) Representative image captured on the smart-phone under dual-wavelength illumination. The left cuvette (control) contained a mixture of Au NPs (0.64 nM) and aptamer (30 nM), while the right cuvette (sample) contained a mixture of Au NPs and aptamer plus 500 nM Hg<sup>2+</sup> (representative of a contaminated water sample). (c) Flow of image-processing steps to compute normalized green-to-red signal ratio (*i.e.*, normalized G/R signal).

the same smart-phone, which will be detailed in the next section.

**Android-Based Smart Application for Mercury Quantification.** We created a custom-designed Android application that allows for mobile testing and sharing of mercury quantification results. After attaching the colorimetric mercury measurement device onto the smart-phone camera unit (Figure 1), the user can hold the cellphone horizontally and then run mercury tests using this smart application. From the main menu of the application, the user can start a new test, create a device-specific calibration curve, view previously run tests, share the test results, and review the operating instructions (Figure 3a). The user can calibrate the application for attachment-specific variations by imaging, for example, mercury-contaminated control samples at known concentrations (Figure 3b). These calibration curves can be stored and reused by various devices/attachments. After capturing a colorimetric transmission image of the sample, the user can first preview the image on the screen before proceeding to digitally analyze/process it (Figure 3c). The application can also use an image file already stored on the phone memory for processing/testing. After pressing on the "Process" button, the transmission signal ratios between the sample and control regions will be automatically computed on the phone, following the image-processing steps discussed in the previous section. A previously stored calibration curve is used to convert the

calculated signal ratio into the mercury concentration level of the sample (in ppb), and the results are then displayed on the screen of the phone (Figure 3d). The total time taken for calculating the mercury concentration on the Android phone (Samsung Galaxy S II) is <7 s. The final test results can be saved on the phone memory with a stamp of time and GPS coordinates of the test and can also be shared with a secure server for spatiotemporal mapping using, for example, a Google Maps-based interface (Figure 3e). With the same Android application, the results can also be reviewed as a function of time per location using a graph-based interface (Figure 3f).

**Calibration and Specificity Tests.** In our cellphone-based mercury detection platform, each normalized G/R ratio computed from a captured RGB image corresponds to a specific mercury concentration value (ppb). The Android application includes a default calibration curve, which was obtained by measuring the normalized G/R ratios of a set of known concentration mercury(II) solutions ranging from 0 to 5  $\mu$ M (see Figure 4). The values of these normalized G/R ratios increased as the concentration of mercury(II) ions rose above 10 nM and reached saturation at >1000 nM (Figure 4). The signal increase in the 10–1000 nM range is mainly due to the aggregation of Au NPs, which is triggered by the mercury(II) ion concentration. This Au NP aggregation process relatively enhances the extinction at the red wavelength (*e.g.*, 625 nm), while it reduces the extinction at

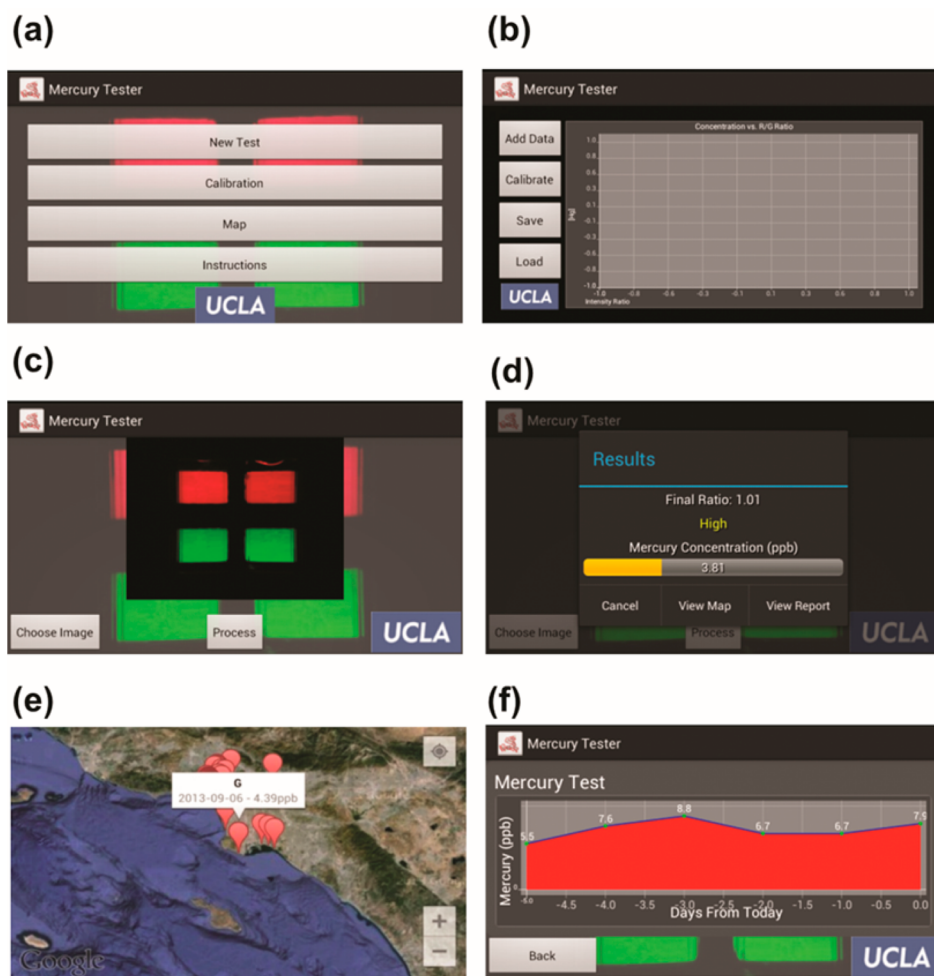


**Figure 3.** Screen shots of our mercury detection application running on an Android phone. (a) Main menu; (b) calibration menu; (c) preview of a captured or selected colorimetric image before proceeding to analyze/quantify the sample; (d) display of the results; (e) spatiotemporal mapping of mercury contamination using a Google Maps-based interface; (f) tracking of mercury levels as a function of time per location.

the green wavelength (e.g., 523 nm), which is also confirmed by our UV-vis spectroscopic measurements (see the Supporting Information, Figure S1a). This plasmon-resonance-based wavelength shift occurred rapidly after around 5 min (Supporting Information, Figure S2), demonstrating a quick response time for the NP/aptamer-based colorimetric assay, making it appropriate for use in field settings. As a result of these plasmonic changes due to NP aggregation, the transmission signal of the red channel relatively decreased, whereas the transmission of the green channel increased. Therefore, the final G/R ratio of a sample increased as the mercury(II) ion concentration is increased, which is also illustrated in the calibration curve presented in Figure 4.

To determine the LOD of our smart-phone-based colorimetric assay, we measured the normalized G/R values of a control sample (*i.e.*,  $[Hg^{2+}] = 0$ ,  $[Au NPs] = 0.64 \text{ nM}$ ,  $[Apt] = 30 \text{ nM}$ ), which resulted in a signal level of  $0.940 \pm 0.025$  ( $\mu_{\text{blank}} \pm \sigma_{\text{blank}}$ ). Our LOD was then determined by the mean of this control sample plus three times its standard deviation ( $\mu_{\text{blank}} + 3\sigma_{\text{blank}}$ ; see

the blue dashed line in Figure 4), which corresponds to a mercury(II) ion concentration of approximately 17.3 nM, or  $\sim 3.5 \text{ ppb}$ . Quite interestingly, the LOD of our smart-phone-based dual-color ratiometric platform was more than 6 times better than the LOD of the exact same assay measured by a portable UV-vis spectrometer (Ocean Optics, HR2000+), which resulted in 123 nM, or 24.6 ppb, LOD (see the Supporting Information, Figure S1b). More importantly, the LOD of mercury(II) ions using our smart-phone-based field-portable sensor has the same order of magnitude as the EPA's mercury(II) reference concentration for drinking water (*i.e.*, 2 ppb)<sup>23</sup> and also satisfies the WHO guideline value for mercury(II) concentration (*i.e.*, 6 ppb).<sup>24</sup>

Next, we performed specificity tests by challenging the same colorimetric plasmonic nanoparticle and aptamer assay with different metal ions, such as  $Fe^{3+}$ ,  $Ca^{2+}$ ,  $Cu^{2+}$ , and  $Pb^{2+}$ , as illustrated in Figure 5. The concentrations of all these metal ion samples were prepared to be 500 nM, and our experiments revealed that, except mercury(II) ions, the other metal

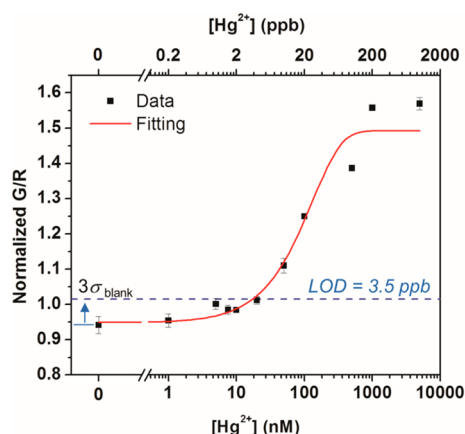


**Figure 4.** Dose-response curve of the Au NP and aptamer based plasmonic colorimetric assay running on a smart-phone. Each measurement at a given concentration was repeated three times. The curve was fitted by an exponential function with a coefficient of determination ( $R^2$ ) of 0.96. An LOD of 3.5 ppb for  $\text{Hg}^{2+}$  was obtained based on the G/R ratios of a control sample ( $[\text{Hg}^{2+}] = 0$ ) plus 3 times the standard deviation of the control (blue dashed line).

ion samples yielded a signal level that is comparable to control samples (Figure 5), verifying the specificity of our assay toward detection of  $\text{Hg}^{2+}$ . The same specificity performance was also confirmed independently by UV-vis spectroscopic measurements as summarized in the Supporting Information, Figure S1c,d.

**Mapping of Mercury Concentration in Water Samples in California.** The performance of our smart-phone-based mercury sensor was also tested with water samples including city tap water and natural water samples collected at over 50 different locations in California. Figure 6 summarizes our measurement results for 19 of these samples collected from various apartments (tap water), rivers, lakes, and beaches on the California coast. The results suggest that all the city tap water samples have undetectable levels of mercury(II) ions since the signal readings are at the same level as our LOD (Figure 6). However, our measurements for the water samples collected from natural sources reveal higher mercury concentration levels, ranging from 3.7 to 8.6 ppb, as illustrated in Figure 6. The samples that are found to contain mercury(II) ion concentrations above 6 ppb, *i.e.*, the safety level recommended by WHO,<sup>24</sup> are mostly from ocean samples, with the worst being from the San Francisco Bay (Figure 6). Our observation that the mercury content in ocean water samples is higher compared to fresh water is probably because the ocean is at the end of mercury's global transport pathway in the environment<sup>52</sup> and thus might exhibit higher pollution levels.

As one of its major advantages, our hand-held smart-phone-based mercury detection platform is also able to generate spatiotemporal contamination maps for, for example, environmental monitoring. To do so, GPS coordinates were recorded for each water sample that was tested, and all the other sample-related

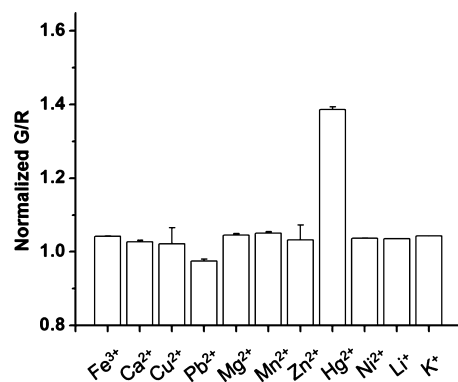


**Figure 5.** Specificity tests of the Au NP and aptamer based plasmonic mercury assay for different metal ions (500 nM). Each measurement was repeated three times.

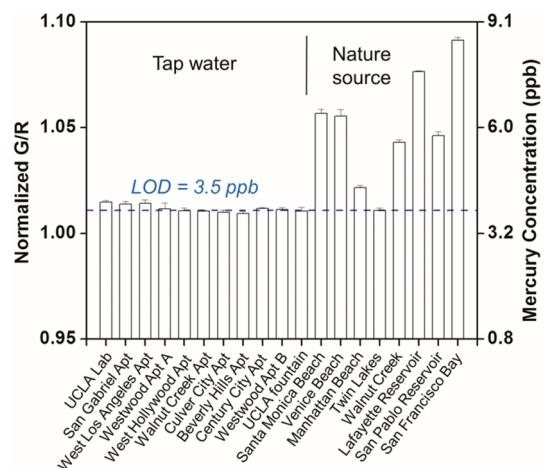


**Figure 6.** Smart-phone-based mercury detection results for 11 tap water samples and eight natural samples collected in California, USA. Each measurement was repeated three times. Note that the measurements are plotted against the G/R ratios, which makes the presented scale of the mercury concentration (ppb) nonlinear, between 0.8 and 9.1 ppb.

information such as measurement results and dates was sent to a secure server using the smart-phone application for mapping of the results. Figure 7a–c represent three smart-phone-generated mercury-monitoring maps, where the spatial resolution of the maps is determined by the sampling density. For instance, in Figure 7a, samples were collected and measured at a low density of ~0.2 measurements/km; in Figure 7b and c, higher resolution was shown by increasing the sampling density to 3.3 and 20 measurements/km, respectively. Figure 7d–f show histogram plots corresponding to the mercury(II) concentrations that are displayed in Figure 7a–c with a better visualization of the variation of mercury(II) levels within a given area. Interestingly, some locations such as points B and C in Figure 7a and d had statistically higher mercury(II) levels than the rest with very small  $p$  values ( $<0.001$ ) determined by standard Student's  $t$  test. Further investigation of this area indicated that the red ROI in Figure 7a included a marina hosting yachts

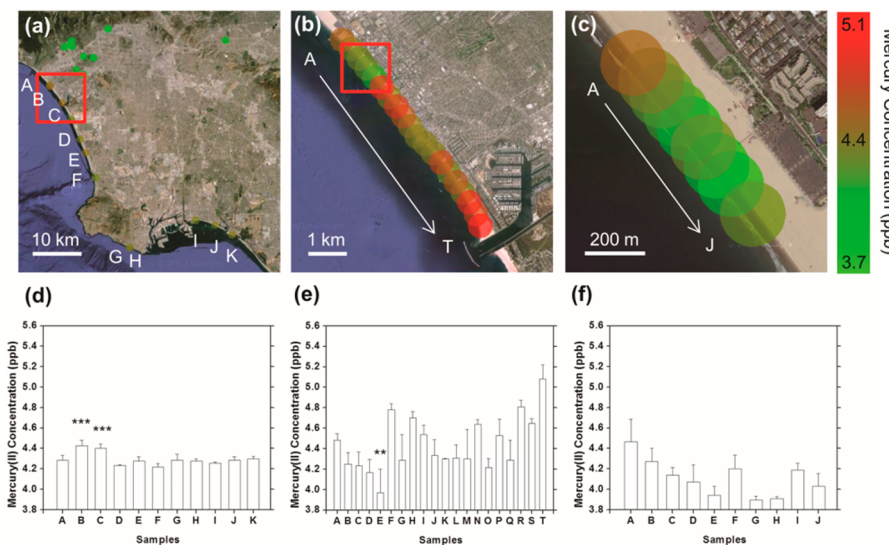


**Figure 7.** Spatiotemporal mapping of mercury contamination in Los Angeles coastal area. (a–c) Geospatial mercury concentration maps with different sampling densities; (b) zoomed-in area of the red ROI in (a); (c) enlarged region of the red ROI in (b). (d–f) Corresponding mercury concentration readings in (a)–(c). All the data points were measured three times.  $p$  values were calculated via two-sample Student's  $t$  test by setting target data set as one population and the rest of the data sets as the other. \*\* represents  $p < 0.01$ , and \*\*\* represents  $p < 0.001$ .

and boats (Figure 7b), which possibly form the major source of heavy metal pollution in that particular region. Mercury(II) ion concentration near the marina also formed a weak gradient (from A to T), as illustrated in Figure 7b and e, with the closest point to the marina having the highest mercury(II) concentration (*i.e.*, point T in Figure 7b and e). Point E in Figure 7e was statistically lower in mercury(II) concentration ( $p < 0.01$ ) compared to other locations within the same region of interest, and this observation was confirmed by higher resolution mercury(II) mapping in Figure 7c and f. In addition to spatial mapping of contamination, the option of monitoring the level of mercury concentration as a function of time for a specific location is also feasible using our smart-phone-based sensing platform as illustrated in Figure 3f.

## CONCLUSIONS

In summary, we introduced a sensitive and cost-effective smart-phone-based mercury(II) ion sensor platform, which utilizes a battery-powered opto-mechanical

reader attached to the existing camera module of a smart-phone to digitally quantify mercury concentration using a plasmonic Au NP and aptamer based colorimetric assay. We employed a two-color ratiometric detection method using LEDs at 523 and 625 nm and a custom-developed Android application for rapid digital image processing of the captured transmission images on the same phone. The LOD of mercury(II) ions with this mobile device is found to be 3.5 ppb, which is on the same order of magnitude with the maximum allowable level of mercury(II) ions in drinkable water defined by the U.S. EPA (2 ppb)<sup>23</sup> and WHO (6 ppb).<sup>24</sup> Moreover, we generated a geospatial mercury(II) contamination map by measuring more than 50 samples collected in California from various sources including tap, river, lake, and ocean water samples. The cost-effective design, portability, and data connectivity of this sensitive heavy metal detection device integrated onto cell-phones could be rather useful for distributed sensing, tracking, and sharing of water contamination information as a function of both space and time, globally.

## METHODS

**Hardware Design.** Our optical imaging system was designed for an Android phone (Samsung Galaxy S II) in Autodesk (Inventor) and printed using a 3D printer (Elite, Dimension). Two LEDs (120 degree illumination angle, SuperBrightLEDs), one green (523 nm, RL5-G16120) and one red (625 nm, RL5-G12120), illuminated the test/sample and control cuvettes simultaneously and were powered by two button cells (3 V, CR1620, Energizer). An optical diffuser (made using three sheets of A4 printer paper) was inserted between the LEDs and the cuvettes for uniform illumination of each cuvette. The transmitted light through the cuvettes was then collected by a plano-convex lens (focal length  $f = 28$  mm, NT65–576, Edmund

Optics) and imaged using the smart-phone camera ( $f = 4$  mm). This imaging configuration provides an optical demagnification factor of  $28/4 = 7$ -fold, which permits imaging of both the test and control cuvettes ( $6.6 \times 6.6$  mm in cross section) within the field of view of the phone's CMOS imager chip. To avoid crosstalk of the two-color illumination, a black clapboard was used to separate the light paths of the LEDs before entering the cuvettes, and four rectangular apertures ( $6.6 \times 5$  mm) were added both in front of and behind the cuvettes to spatially filter the transmitted light at each color (*i.e.*, red and green). The acquired images were analyzed in digitally separated red and green channels to further reject possible spectral crosstalk between red and green illumination wavelengths.

**Gold Nanoparticle and Aptamer Based Colorimetric Assay.** Citrate-stabilized Au NPs (50 nm) were purchased from NanoComposix. Aptamer sequence of 5'-TTTTTTTTT-3' was obtained from Integrated DNA Technologies. All metal salts such as mercury(II) chloride were obtained from Sigma. Stock Au NP solution in 20 mM Tris-HCl buffer (TH, pH 8.0) was prepared by centrifugation of raw Au NP-citrate solution, aspiration of the supernatant, and redispersion in TH buffer with 20× dilution to give a working concentration of 0.64 nM. Water samples collected from rivers, lakes, and beaches were filtered by a 0.2 μm polyethersulfone membrane (Whatman) to remove sand and other solid particles within the test samples. Tap water samples and calibration solutions containing mercury(II) ions prepared in deionized water were used directly without further purification. In a typical measurement procedure, 4 μL of the sample of interest was mixed with 4 μL of 3 μM aptamer (20 mM TH buffer, pH 8.0), followed by a 5 min reaction period. Next, 400 μL of Au NPs (0.64 nM) in 20 mM TH buffer solution was added and allowed to react for 5 min. Finally, 8 μL of 10 mM NaCl was added and incubated for another 10 min before being analyzed by the smart-phone device.

**UV–Vis Spectroscopic Investigation of Water Samples Using a Portable Spectrometer.** In our comparison measurements against the smart-phone (see the Supporting Information), a white LED (RL5-W15120, SuperBrightLEDs) was used as the light source, and the transmission signal that passed through a standard 1 cm cuvette was collected by a 600-μm-diameter optical fiber and measured by a portable spectrometer (HR2000+, Ocean Optics). The background spectrum was recorded using deionized water as a blank control sample. Each spectrum was collected with an exposure time of 1 ms and scanned 500 times for averaging in order to improve the signal-to-noise ratio of each UV–vis spectroscopic measurement.

**Conflict of Interest:** The authors declare the following competing financial interest(s): A. Ozcan is the cofounder of a start-up company that aims to commercialize computational microscopy tools.

**Acknowledgment.** Ozcan Research Group gratefully acknowledges the support of the Presidential Early Career Award for Scientists and Engineers (PECASE), Army Research Office (ARO) Life Sciences Division, ARO Young Investigator Award, National Science Foundation (NSF) CAREER Award, NSF CBET Division Biophotonics Program, NSF Emerging Frontiers in Research and Innovation (EFRI) Award, Office of Naval Research (ONR), and National Institutes of Health (NIH) Director's New Innovator Award DP2OD006427 from the Office of the Director, National Institutes of Health. We also thank Dr. Hangfei Qi from Prof. Ren Sun's lab at the Department of Molecular and Medical Pharmacology (UCLA) for providing the aptamer sequence.

**Supporting Information Available:** UV–vis spectroscopic measurement results of the Au NP and aptamer based colorimetric assay (calibration curve, specificity, and dynamics test). This material is available free of charge via the Internet at <http://pubs.acs.org>.

## REFERENCES AND NOTES

- International Programme on Chemical Safety (IPCS). *Methylmercury*; World Health Organization, 1990. <http://www.inchem.org/documents/ehc/ehc/ehc101.htm>.
- Tsubaki, T. *Minamata Disease: Methylmercury Poisoning in Minamata and Niigata, Japan*; Elsevier Scientific: Amsterdam, 1977.
- Harada, M. *Minamata Disease: Methylmercury Poisoning in Japan Caused by Environmental Pollution*. *Crit. Rev. Toxicol.* **1995**, *25*, 1–24.
- TEACH. *Organic Mercury*, U.S. Environmental Protection Agency, 2007. [http://www.epa.gov/teach/chem\\_summ/mercury\\_org\\_summary.pdf](http://www.epa.gov/teach/chem_summ/mercury_org_summary.pdf).
- Clarkson, T. W. *The Toxicology of Mercury*. *Crit. Rev. Clin. Lab. Sci.* **1997**, *34*, 369–403.
- Wolfe, M. F.; Schwarzbach, S.; Sulaiman, R. A. Effects of Mercury on Wildlife: A Comprehensive Review. *Environ. Toxicol. Chem.* **1998**, *17*, 146–160.
- TEACH. *Inorganic Mercury*, U.S. Environmental Protection Agency, 2007. [http://www.epa.gov/teach/chem\\_summ/mercury\\_inorg\\_summary.pdf](http://www.epa.gov/teach/chem_summ/mercury_inorg_summary.pdf).
- Blum, J. D.; Popp, B. N.; Drazen, J. C.; Anela Choy, C.; Johnson, M. W. Methylmercury Production below the Mixed Layer in the North Pacific Ocean. *Nat. Geosci.* **2013**, *6*, 879–884.
- Stacchiotti, A.; Morandini, F.; Bettoni, F.; Schena, I.; Lavazza, A.; Grigolato, P. G.; Apostoli, P.; Rezzani, R.; Aleo, M. F. Stress Proteins and Oxidative Damage in a Renal Derived Cell Line Exposed to Inorganic Mercury and Lead. *Toxicology* **2009**, *264*, 215–224.
- Harnly, M.; Seidel, S.; Rojas, P.; Fornes, R.; Flessel, P.; Smith, D.; Kreutzer, R.; Goldman, L. Biological Monitoring for Mercury within a Community with Soil and Fish Contamination. *Environ. Health Perspect.* **1997**, *105*, 424–429.
- Legrand, M.; Sousa Passos, C. J.; Mergler, D.; Chan, H. M. Biomonitoring of Mercury Exposure with Single Human Hair Strand. *Environ. Sci. Technol.* **2005**, *39*, 4594–4598.
- Hightower, J. M.; Moore, D. Mercury Levels in High-End Consumers of Fish. *Environ. Health Perspect.* **2003**, *111*, 604–608.
- McDowell, M. A.; Dillon, C. F.; Osterloh, J.; Bolger, P. M.; Pellizzari, E.; Fernando, R.; de Oca, R. M.; Schober, S. E.; Sinks, T.; Jones, R. L.; et al. Hair Mercury Levels in U.S. Children and Women of Childbearing Age: Reference Range Data from NHANES 1999–2000. *Environ. Health Perspect.* **2004**, *112*, 1165–1171.
- Lee, J.-S.; Mirkin, C. A. Chip-Based Scanometric Detection of Mercuric Ion Using DNA-Functionalized Gold Nanoparticles. *Anal. Chem.* **2008**, *80*, 6805–6808.
- Cho, E. S.; Kim, J.; Tejerina, B.; Hermans, T. M.; Jiang, H.; Nakanishi, H.; Yu, M.; Patashinski, A. Z.; Glotzer, S. C.; Stellacci, F.; et al. Ultrasensitive Detection of Toxic Cations through Changes in the Tunnelling Current across Films of Striped Nanoparticles. *Nat. Mater.* **2012**, *11*, 978–985.
- Gartia, M. R.; Braunschweig, B.; Chang, T.-W.; Moinzadeh, P.; Minsker, B. S.; Agha, G.; Wieckowski, A.; Keefer, L. L.; Liu, G. L. The Microelectronic Wireless Nitrate Sensor Network for Environmental Water Monitoring. *J. Environ. Monit.* **2012**, *14*, 3068–3075.
- Lafleur, J. P.; Senkbeil, S.; Jensen, T. G.; Kutter, J. P. Gold Nanoparticle-Based Optical Microfluidic Sensors for Analysis of Environmental Pollutants. *Lab Chip* **2012**, *12*, 4651–4656.
- Chung, E.; Gao, R.; Ko, J.; Choi, N.; Lim, D. W.; Lee, E. K.; Chang, S.-I.; Choo, J. Trace Analysis of Mercury(II) Ions Using Aptamer-Modified Au/Ag Core-Shell Nanoparticles and SERS Spectroscopy in a Microdroplet Channel. *Lab Chip* **2013**, *13*, 260–266.
- Lin, Y.-W.; Huang, C.-C.; Chang, H.-T. Gold Nanoparticle Probes for the Detection of Mercury, Lead and Copper Ions. *Analyst* **2011**, *136*, 863–871.
- Liu, D.; Wang, Z.; Jiang, X. Gold Nanoparticles for the Colorimetric and Fluorescent Detection of Ions and Small Organic Molecules. *Nanoscale* **2011**, *3*, 1421–1433.
- Du, J.; Jiang, L.; Shao, Q.; Liu, X.; Marks, R. S.; Ma, J.; Chen, X. Colorimetric Detection of Mercury Ions Based on Plasmonic Nanoparticles. *Small* **2013**, *9*, 1467–1481.
- El Kaoutit, H.; Estévez, P.; García, F. C.; Serna, F.; García, J. M. Sub-ppm Quantification of Hg(II) in Aqueous Media Using Both the Naked Eye and Digital Information from Pictures of a Colorimetric Sensory Polymer Membrane Taken with the Digital Camera of a Conventional Mobile Phone. *Anal. Methods* **2013**, *5*, 54–58.
- U.S. EPA. *National Primary Drinking Water Regulations*. US EPA, 2009. <http://water.epa.gov/drink/contaminants/index.cfm#list>.
- World Health Organization. *Guidelines for Drinking Water Quality*, 4th ed.; World Health Organization: Geneva, **2011**. [http://whqlibdoc.who.int/publications/2011/9789241548151\\_eng.pdf](http://whqlibdoc.who.int/publications/2011/9789241548151_eng.pdf).

25. Vashist, S.; Mudanyali, O.; Schneider, E. M.; Zengerle, R.; Ozcan, A. Cellphone-Based Devices for Bioanalytical Sciences. *Anal. Bioanal. Chem.* **2013**, *10*.1007/s00216-013-7473-1.
26. Coskun, A. F.; Ozcan, A. Computational Imaging, Sensing and Diagnostics for Global Health Applications. *Curr. Opin. Biotechnol.* **2013**, *25*, 8–16.
27. Tseng, D.; Mudanyali, O.; Oztoprak, C.; Isikman, S. O.; Sencan, I.; Yaglidere, O.; Ozcan, A. Lensfree Microscopy on Cellphone. *Lab Chip* **2010**, *10*, 1787–1792.
28. Zhu, H.; Mavandadi, S.; Coskun, A. F.; Yaglidere, O.; Ozcan, A. Optofluidic Fluorescent Imaging Cytometry on a Cell Phone. *Anal. Chem.* **2011**, *83*, 6641–6647.
29. Zhu, H.; Yaglidere, O.; Su, T.-W.; Tseng, D.; Ozcan, A. Cost-Effective and Compact Wide-Field Fluorescent Imaging on a Cell-Phone. *Lab Chip* **2011**, *11*, 315–322.
30. Preechaburana, P.; Gonzalez, M. C.; Suska, A.; Filippini, D. Surface Plasmon Resonance Chemical Sensing on Cell Phones. *Angew. Chem., Int. Ed.* **2012**, *51*, 11585–11588.
31. Shen, L.; Hagen, J. A.; Papautsky, I. Point-of-Care Colorimetric Detection with a Smartphone. *Lab Chip* **2012**, *12*, 4240–4243.
32. Mudanyali, O.; Dimitrov, S.; Sikora, U.; Padmanabhan, S.; Navruz, I.; Ozcan, A. Integrated Rapid-Diagnostic-Test Reader Platform on a Cellphone. *Lab Chip* **2012**, *12*, 2678–2686.
33. Zhu, H.; Sikora, U.; Ozcan, A. Quantum Dot Enabled Detection of Escherichia coli Using a Cell-Phone. *Analyst* **2012**, *137*, 2541–2544.
34. Gallegos, D.; Long, K. D.; Yu, H.; Clark, P. P.; Lin, Y.; George, S.; Nath, P.; Cunningham, B. T. Label-Free Biodetection Using a Smartphone. *Lab Chip* **2013**, *13*, 2124–2132.
35. O'Driscoll, S.; MacCraith, B. D.; Burke, C. S. A Novel Camera Phone-Based Platform for Quantitative Fluorescence Sensing. *Anal. Methods* **2013**, *5*, 1904–1908.
36. Oncescu, V.; O'Dell, D.; Erickson, D. Smartphone Based Health Accessory for Colorimetric Detection of Biomarkers in Sweat and Saliva. *Lab Chip* **2013**, *13*, 3232–3238.
37. Lillehoj, P. B.; Huang, M.-C.; Truong, N.; Ho, C.-M. Rapid Electrochemical Detection on a Mobile Phone. *Lab Chip* **2013**, *13*, 2950–2955.
38. Zhu, H.; Sencan, I.; Wong, J.; Dimitrov, S.; Tseng, D.; Nagashima, K.; Ozcan, A. Cost-Effective and Rapid Blood Analysis on a Cell-Phone. *Lab Chip* **2013**, *13*, 1282–1288.
39. Coskun, A. F.; Nagi, R.; Sadeghi, K.; Phillips, S.; Ozcan, A. Albumin Testing in Urine Using a Smart-Phone. *Lab Chip* **2013**, *13*, 4231–4238.
40. Coskun, A. F.; Wong, J.; Khodadadi, D.; Nagi, R.; Tey, A.; Ozcan, A. A Personalized Food Allergen Testing Platform on a Cellphone. *Lab Chip* **2013**, *13*, 636–640.
41. Navruz, I.; Coskun, A. F.; Wong, J.; Mohammad, S.; Tseng, D.; Nagi, R.; Phillips, S.; Ozcan, A. Smart-Phone Based Computational Microscopy Using Multi-Frame Contact Imaging on a Fiber-Optic Array. *Lab Chip* **2013**, *13*, 4015–4023.
42. Wei, Q.; Qi, H.; Luo, W.; Tseng, D.; Ki, S. J.; Wan, Z.; Göröcs, Z.; Bentolila, L. A.; Wu, T.-T.; Sun, R.; et al. Fluorescent Imaging of Single Nanoparticles and Viruses on a Smart Phone. *ACS Nano* **2013**, *7*, 9147–9155.
43. Portio Research Limited. *Portio Research Mobile Factbook* 2013. <http://www.portioresearch.com/media/3986/Portio%20Research%20Mobile%20Factbook%202013.pdf>.
44. Kim, Y.; Johnson, R. C.; Hupp, J. T. Gold Nanoparticle-Based Sensing of "Spectroscopically Silent" Heavy Metal Ions. *Nano Lett.* **2001**, *1*, 165–167.
45. Lee, J.-S.; Han, M. S.; Mirkin, C. A. Colorimetric Detection of Mercuric Ion ( $Hg^{2+}$ ) in Aqueous Media Using DNA-Functionalized Gold Nanoparticles. *Angew. Chem., Int. Ed.* **2007**, *46*, 4093–4096.
46. Huang, C.-C.; Chang, H.-T. Parameters for Selective Colorimetric Sensing of Mercury(II) in Aqueous Solutions Using Mercaptopropionic Acid-Modified Gold Nanoparticles. *Chem. Commun.* **2007**, 1215–1217.
47. Darbha, G. K.; Singh, A. K.; Rai, U. S.; Yu, E.; Yu, H.; Chandra Ray, P. Selective Detection of Mercury(II) Ion Using Non-linear Optical Properties of Gold Nanoparticles. *J. Am. Chem. Soc.* **2008**, *130*, 8038–8043.
48. Liu, D.; Wang, S.; Swierczewska, M.; Huang, X.; Bhirde, A. A.; Sun, J.; Wang, Z.; Yang, M.; Jiang, X.; Chen, X. Highly Robust, Recyclable Displacement Assay for Mercuric Ions in Aqueous Solutions and Living Cells. *ACS Nano* **2012**, *6*, 10999–11008.
49. Li, L.; Li, B.; Qi, Y.; Jin, Y. Label-Free Aptamer-Based Colorimetric Detection of Mercury Ions in Aqueous Media Using Unmodified Gold Nanoparticles as Colorimetric Probe. *Anal. Bioanal. Chem.* **2009**, *393*, 2051–2057.
50. Miyake, Y.; Togashi, H.; Tashiro, M.; Yamaguchi, H.; Oda, S.; Kudo, M.; Tanaka, Y.; Kondo, Y.; Sawa, R.; Fujimoto, T.; et al. Mercuryll-Mediated Formation of Thymine-HgII-Thymine Base Pairs in DNA Duplexes. *J. Am. Chem. Soc.* **2006**, *128*, 2172–2173.
51. Tanaka, Y.; Oda, S.; Yamaguchi, H.; Kondo, Y.; Kojima, C.; Ono, A. 15n-15n J-Coupling across HgII: Direct Observation of HgII-Mediated T-T Base Pairs in a DNA Duplex. *J. Am. Chem. Soc.* **2006**, *129*, 244–245.
52. Boening, D. W. Ecological Effects, Transport, and Fate of Mercury: A General Review. *Chemosphere* **2000**, *40*, 1335–1351.